3. PARTICIPATION IN THE USE OF THE JET FACILITIES BY THE EFDA ASSOCIATES

F. Serra (Head), D. Borba, C. Correia, L. Cupido, M.E. Manso, M.F. Nave, C. Silva, C. Varandas, M.P. Alonso, P. Belo, R. Coelho, S. Cortes, N. Cruz, L. Meneses, F. Nabais, I. Nunes, R.C. Pereira, T. Ribeiro

3.1. INTRODUCTION

The Association EURATOM/IST has participated during 2000 in the use of the JET Facilities by the Associates, in the frame of the “European Fusion Development Agreement” through the “JET Operation Contract” and the “JET Implementing Agreement”.

This chapter presents the main activities carried out during this year in the areas of operation, scientific exploitation and management.

3.2. OPERATION

3.2.1. Introduction

Table 3.1 contains some administrative details concerning the participation of Portuguese engineers in the JET Operation Team, through Secondments Agreements with the Association EURATOM/ UKAEA.

Mr. Santiago Cortes has been working in the Motional Stark Effect (MSE) Diagnostic Group. The main activities performed in 2000 have been:

- Installation of a new optical system
- Calibration and improvement of the spectral resolution of the survey spectrometer.
- Calibration of the device for the incoming un-polarized light.
- Analysis of data from the campaigns C1, C2 and C3.

Mr. Luis Meneses has been working in the Reflectometry and LIDAR Diagnostics Groups. The main activities carried out in 2000 have been:

- Testing, calibration and installation of a reflectometry (KG8a) operating in X-mode for density profile measurements (50-70 GHz).
- Design of new electronics for the generator of the KG8a reflectometer.
- Testing, calibration and installation of a correlation reflectometer (KG3c) with one channel operating in O-mode at 33-34 GHz.
- Analysis of the experimental results and study of further improvements on these diagnostics.

3.2.2. Motional stark effect diagnostic

The Motional Stark Effect diagnostic at JET relies on the Stark splitting of the D_α (656.3 nm) emission line from the neutral deuterium particles injected into the plasma with high velocity (3×10^6 ms^{-1}) crossing the magnetic field, experience a motional electric field of around 5 MV m^{-1}. This emission has two polarized orthogonal components, σ and π, being this polarization either perpendicular or parallel to the motional electric field respectively. By measuring the state of polarization of one of these components it is possible to measure the pitch angle γ_m. Then, the local pitch angle is given by the measured pitch angle corrected from a geometric factor. Using an equilibrium reconstruction code, like EFIT, the density current distribution profile j(r) is readily calculated.

Fig. 3.1 shows the conceptual layout of the diagnostic. The emitted light from the heating beams is collected by a periscope using an Amici prism and is carried out to the polarimeter by a lens system with low Verdet constant to avoid unwanted induced polarization through the Faraday effect. The polarimeter consists of two photo-elastic modulators (PEMs) in tandem with a polarization analyser. The

Name	Category	Area	Beginning	Days
Luis Meneses	Research Assistant	Microwave Diagnostics	01.02.00	289.5
Santiago Cortes	Research Assistant	Spectroscopy	03.01.00	311.5

Table 3.1 – Portuguese participation in the JET Operation Contract

polarization direction is encoded as amplitude modulation of the detector signals at harmonics of the PEM modulation frequencies. The modulated light is conveyed by fibre optics to a remote detection system. The desired Stark component is spectrally resolved by a set of 25 double cavity interference filters, with 0.4 nm band-pass, each one corresponding to a MSE channel. In front of the interference filters there is an aspheric optic system that focuses the light onto an avalanche photodiode detector (APD). Data is digitised and signal processing is performed to extract the required harmonic frequencies. A survey spectrometer in a Czerny-Turner configuration is attached to the MSE lines of sight to aid in setting the required wavelenghts.

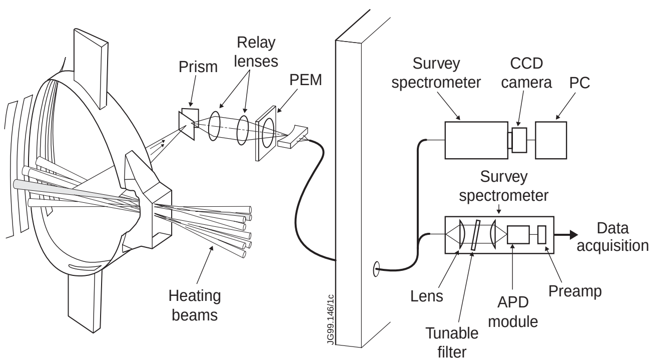

Fig. 3.1 – The JET Motional Stark Effect diagnostic

3.3. SCIENTIFIC EXPLOITATION

3.3.1. Introduction

Table 3.2 summarizes the Portuguese participation in the scientific exploitation of the JET Facilities. The activities have been performed in the frame of S/T Orders and Notifications (N).

3.3.2. MHD studies

3.3.2.1. Introduction

The activity in this research area has been focussed in the following topics:

- MHD activity and loss of confinement in JET radiative mantle experiments
- Influence of sawtooth pre-cursors at the onset of neo-classical tearing modes
- Effect of plasma rotation on sawtooth stabilization by neutral beam injection
- Internal kink stability analysis of JET impurity seeded discharges

3.3.2.2. MHD activity and loss of confinement in JET radiative mantle experiments

The study of plasmas with radiating edges is one of the main research topics of the JET-EFDA Task Force S1. Argon seeded plasmas in a variety of plasma configurations produced high confinement H-modes with densities close to the Greenwald limit. In the septum configuration, the highest performance radiative mantle plasmas, ($H_{97}*f_{GWD} \geq 0.8$) were obtained with two gas injection phases: an initial phase of continuous D_2 and Ar fuelling, followed by the "after-glow" phase when both gases injection rates are reduced. In discharges with low or moderate Ar seeding, a quasi-steady state regime remains through to the end of the applied heating.

However, at high Ar injection rates ($\geq 8x10^{21}$ el/s), the high confinement phase is transient. Analysis of bolometry data indicates that confinement degradation occurs when Ar accumulates in the plasma core. This degradation correlates with disappearance of sawtooth activity (Fig. 3.2). Usually, the central Ar density increases when the amplitude of sawteeth crashes decreases. A sudden increase in central impurity concentration follows when the sawtooth activity is suppressed.

Type	Name	Category	Task Force	From/to	Days
S/T	Peres Alonso	Research Assistant	D-1	17/05/00 to 12/11/00	175
S/T	Carlos Silva	Assistant Research	D-9, E-1	23/10/00 to 09/12/00	49
S/T	Filomena Nave	Assistant Research	M-1, M-2, M-4, M-5, S1-3	06/06/00 to 28/07/00 30/08/00 to 08/12/00	211
S/T	Tiago Ribeiro	Research Assistant	D-2, M-3	24/06/00 to 30/09/00	65
N	Fernando Nabais	Research Assistant	M	19/09/00 to 15/12/00	88
N	Paula Belo	Research Assistant	M	18/09/00 to 15/12/00	89
S/T	Luis Meneses	Research Assistant	D	01/02/00 to 31/12/00	34.5
S/T	Santiago Cortes	Research Assistant	D	03/01/00 to 31/12/00	51.5
S/T	Luis Cupido	Assistant Research	D		10

Table 3.2 – Portuguese participation in the scientific exploitation

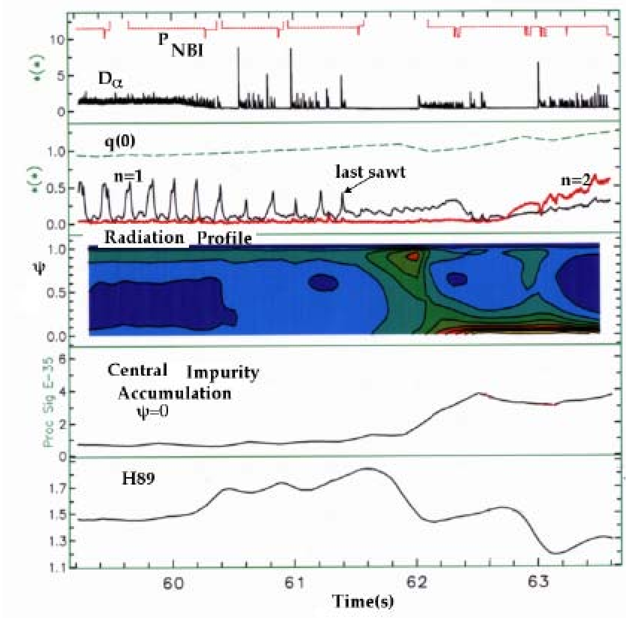

Fig. 3.2 - Discharge with large Argon density. The after-glow phase starts at 60s, q(0) starts to increase and reaches values above unity. The amplitude of the n=1 sawtooth precursors decrease and at ~61.5 s sawtooth activity stops. The contour plot of the radiation profiles shows an increase of the radiation in the central regions (Ψ>0.5). The impurity concentration in the centre (Ψ~0) also increases. The confinement factor H89 shows that the confinement decreases.

Sawtooth behaviour was found to depend on the Deuterium and Ar densities and the evolution of q(0). In particular, the q-profiles calculated with EFIT indicate that q(0) in the afterglow phase increases, reaching values above unity. In order to keep q(0) below the unity, two types of experiments were performed: a) programming of the q-profile, by designing discharges at different plasma currents and magnetic fields; and b) heating the plasma on axis with ICRF. The latter proved to be a successful method to improve q (0) stationarity. A small amount of ICRF power (3 MW) was used in discharges with low Ar concentrations. This increased the electron temperature on axis, thus preventing the increase of q(0) and maintaining sawtooth. In experiments planed for the JET campaign C4 (2001), ICRF heating will be used in discharges with high Ar concentrations. The ICRH power and RF phasing will be tuned to minimise fast particle stabilisation.

3.3.2.3. Amplitude of sawtooth precursors at the onset of neo-classical tearing modes

The JET 2000 experimental campaign provided an extensive database of Neo-Classical Tearing Mode (NTM) observations in ELMy H-modes. In most cases the onset of NTMs appears to be associated to sawtooth MHD activity and specially designed experiments have shown that increasing the frequency of sawtooth crashes the onset of NTMs is delayed. In order to understand the role that the sawtooth plays on seed island creation, the amplitude of sawtooth precursors at the time a (3,2) NTM is triggered is being studied. At JET, sawtooth precursor oscillations at moderate normalised beta values, β_N ~2-3.5, are long-lived continuous oscillations, present during most of the sawtooth temperature ramp up. The onset of a NTM is usually observed at or before a sawtooth crash as the n=1 precursor reaches maximum amplitude. This suggests that the NTM seed island may be determined either by non-linear coupling with the n=1 component or by toroidal coupling with the n=2 component of the sawtooth precursor. The subsequent sawtooth crash would then provide conditions for further destabilisation and growth of the NTM. In order to test experimentally the mode-coupling hypothesis, it is important to determine the ratio of amplitudes of sawtooth precursor to NTM seed island. Preliminary analysis show that the n=1 amplitude at time of NTM onset is found to increase as β_N^{α} , where $\alpha>1$(Fig. 3.3), which would increase the sensitivity of the NTM onset on the seed island formation at high β_N. However, the required n=1 amplitude for the NTM onset appears to depend on the heating method used, such as the position of the ion-cyclotron radio frequency (ICRF) resonance position with respect to the q=1 position and the ICRF phasing.

3.3.2.4. Effect of plasma rotation on sawtooth stabilization by neutral beam injection[1]

Sawtooth stabilisation by NBI ions is not clearly understood, since NBI ions are usually not ``fast'' enough to stabilise the m=1 internal kink mode which is believed to cause the sawtooth crash. JET experiments, on the order hand, show quite clear that the sawtooth period and the sawtooth crash amplitude increase with NBI power. In order to understand the observed sawtooth stabilisation in tokamak experiments with NBI heating, the internal kink mode stability of JET plasmas was modelled using three codes developed at Princeton Plasma

[1] In collaboration with Princeton Plasma Physics Laboratory (PPPL), N.J., U.S.A.

Physics Laboratory: two versions of the code NOVA and the non-linear code M3D.

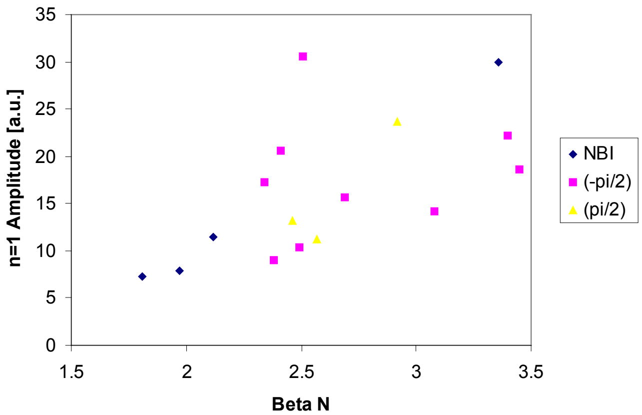

Fig. 3.3 - Amplitude of n=1 sawtooth precursor at the time of onset of (3,2) NTMs in a JET experiment designed to control sawtooth behaviour, measured in discharges with 3 different heating schemes: NBI, ICRF with phase $-\pi/2$ and ICRF with phase $+\pi/2$. It shows that the n=1 amplitude increases with the normalised beta value. The reason for large spread in the data is being investigated. It appears to depend on details of the heating scheme used.

The three codes were benchmarked and produce good agreement, for one baseline tokamak equilibrium. In addition, plasma sheared rotation has been introduced in the calculations. The three codes were then used to analyse JET ELM-free Deuterium and Deuterium-Tritium plasmas. Input for the MHD calculations is taken from the transport code TRANSP. In the NOVA-K analysis the m=1 mode is assumed to rotate with a frequency equal to the plasma rotation frequency at the q=1 surface while it has a global structure and can interact with fast particles at different minor radii. For JET high performance hot-ion H-modes, the effect of the plasma rotation was modelled by prescribing a toroidal co-current rotation velocity in the form $\Omega_\varphi = [a(1-\varphi)^{0.75} + b].10^5 rad^{-1}$. The effect of rotation on the different fast particle species was studied by introducing the rotation enhancement factor as shown in the figure. The stabilisation of the (1,1) mode is sensitive to the toroidal sheared rotation if its toroidal precession is comparable with the variation of the rotation within the q=1 surface $\omega_{d\varphi} \sim r\partial\Omega_\varphi / \partial r$. Hence the rotation is less important for ICRH ions and alpha particles then for beam ions, which have much smaller precession frequency. The co-rotating plasma with the velocity shear supports the stabilisation effectively because it increases the particle energy by providing extra toroidal precession. In conclusion, rotation was found to increase the fast particle contribution to m=1 stability. Analysis show that with rotation included, the NBI ion contribution to the quadratic form of the m=1 mode makes this mode stable. This result is in qualitative agreement with observations of long sawtooth periods in JET high performance plasmas.

3.3.2.5. Internal kink stability analysis of JET impurity seeded discharges

In recent JET experiments of impurity seeded discharges in the ELMy H-mode regime, ICRF heating was used to control the evolution of the q-profile and to avoid suppression of sawteeth. ICRF heating is a known method to increase the sawtooth period leading to monster sawteeth regimes. Therefore, careful tuning of the ICRF power and resonance position was needed, in order to increase the central electron temperature keeping q(0) below 1, while at the same time avoiding sawtooth stabilisation by fast particles. To help the planning of these experiments, the influence of ICRH-driven hot particles on the internal kink stability was studied using the CASTOR-K code. This code calculates the energy transfer between hot particles and waves, in this case the energy transfer between the ICRF-driven hot particles and the internal kink mode believed to be responsible for the sawtooth. This allows the determination of the contribution of the ICRF-driven energetic particles to the growth rate of the internal kink mode in the linear regime.

Several discharges have been analysed. First, the effect of adding ICRF heating to existing Ar seeded discharges, heated with 10 MW of NBI power, was considered. This allowed a predictive study of the effect of using different heating powers, resonant positions and different ICRF fast particle distributions on the internal kink stability. Once the experiments were performed, the discharges with added ICRF heating were analysed and the result of calculations as well as observational results, were compared with the predictions.

Fig. 3.4 shows the transference of energy between the internal kink mode and the ICRF-driven hot particles, normalised to the mode energy and the Alfven frequency (δW_{HOT}), for discharge #52146.(with P_{NBI}=10MW and P_{ICRF}=3MW). The contribution to the growth rate of the internal kink mode due to the presence of ICRF-driven particles can be calculated from this value. Positive values of the transferred energy (or growth rate) mean that the ICRH-driven fast particles have a destabilising effect, while negative values means that these hot particles contributes to stabilise the wave. Stability depends on the mode frequency (typically 10 kHz in these discharges) and fast particle energy distribution details. In this figure, for each curve a different combination of T_{hot} (fast particles temperature) and / $\lambda=\tilde{\mu}E$ (fast particles pitch angle) was assumed.

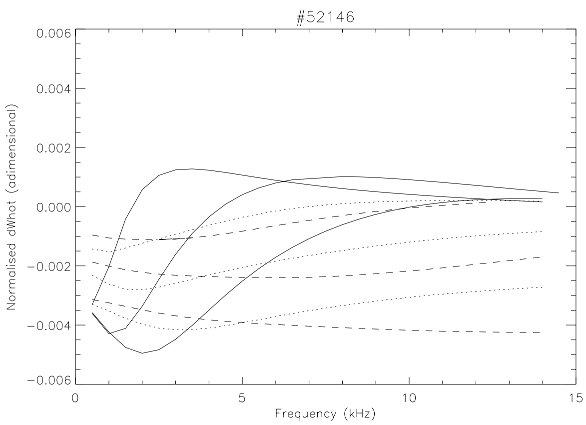

Fig. 3.4 - Energy transferred between the internal kink mode and the ICRH-driven particles as function of the mode frequency. Solid lines, T_{HOT}=40 keV and λ=0.98, 1.00 and 1.02 (starting from the bottom for the lowest frequency). Dotted lines, T_{HOT}=100 keV and λ=0.98, 1.00 and 1.02. Dashed lines T_{HOT}=100 keV and λ=0.98, 1.00 and 1.02. Calculations indicated that for discharge #52146 (T_{HOT}=40 keV, λ=0.98) ICRH-driven particles would have only a very small destabilising effect.

Results of the simulations show that a modest ICRH power applied on axis to discharges with high density plasmas, as the Ar discharges analysed, the ICRF-driven ions (E~50 keV) could not affect significantly the internal kink stability. Any significant transference of energy between the internal kink mode and the ICRH-driven particles would require higher particle energies, that could only be achieved with lower plasma densities or higher ICRH power.

3.3.3. Edge physics

3.3.3.1. Introduction

The activities in this research area have been focused in the following topics:

- Fluctuations measurements using single Langmuir probes
- Fluctuations measurements using a modified triple probe
- Small scale fluctuating sheared E×B flows.

3.3.3.2. Fluctuations measurements using single Langmuir probe characteristics

Fluctuations are responsible for a significant portion of the particle loss rate in tokamaks and may account for a large part of the anomalous energy losses observed. For a complete estimate of the particle and heat transport, knowledge of the fluctuations in density, temperature and electric field are needed. However, temperature fluctuations are in general difficult to measure and then often ignored.

Fluctuations in the Langmuir probe collected current result from fluctuations in plasma quantities (density (*n*), electron temperature (T_e), and floating potential (V_f)). Therefore, the probe characteristic may be used to obtain information from fluctuation in the plasma parameters. One method that, in principle, can resolve all the quantities of interest has been successfully used by D. Robinson for a double probe. It involves studying the variation of the probe current fluctuation as a function of the applied voltage.

The aim of this work is to apply that method to the single probe characteristic in order to obtain information on $\tilde{n}$, $\tilde{T}$, $\tilde{V}_f$ and their cross-correlations. The method consists of fitting the experimentally determined probe current fluctuation level to a theoretical curve as a function of the bias; the required fluctuation levels are the coefficients which are returned by the curve-fitting routine.

We have shown that this method is able to resolve plasma fluctuations using single probe characteristics. This method has been applied to JET reciprocating probe data and results show that temperature fluctuations are, in general, reasonably low. In L-mode plasmas we found that close to the separatrix $\tilde{T}_e/T_e \le 0.5\,\tilde{n}/n \cong 5\,\%$ and $\tilde{V}_f/T_e \cong 25\,\%$, which is in good agreement with results obtained from probes measuring floating potential and ion saturation current. Fig. 3.5 shows a typical example of the collected current fluctuation level as a function of the applied voltage and the resulting fit.

This method is experimentally very simple. It does not involve complex circuitry, rapid sweep voltages or multiple probe configurations, and allows the determination of the fluctuations in plasma quantities with high temporal resolution (acquisition frequency of the current signal) although measurements are not time-resolved (a complete I-V characteristic is needed). Another advantage of the method when compared with double or triple probe method is that it provides local measurements, therefore fluctuations in plasma gradient do not have to be taken into account.

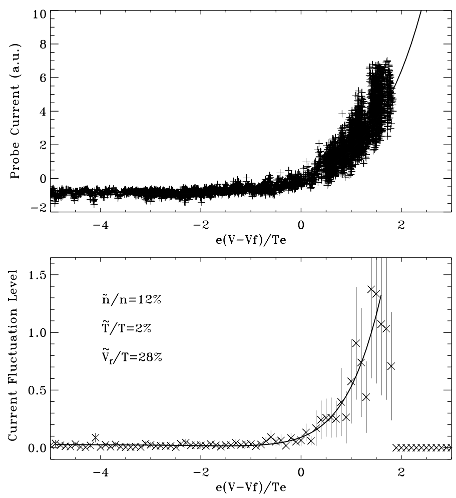

Fig. 3.5 - Typical example of a Langmuir probe characteristic (a) and current fluctuation level as a function of the applied voltage and the resulting fit (b).

3.3.3.3. Temperature fluctuations measurements using a modified triple probe

A new fluctuation probe system is being developed in order to clarify the influence of temperature fluctuations in the total turbulent flux. The new probe consists on a basic modified triple probe system. The effective size of the modified triple probe is 5 mm which is smaller than the typical poloidal correlation length of fluctuations (5-10 mm).

The new fluctuations probe head has been used on a dedicated day for turbulence studies with the aim of measuring turbulent fluxes and testing the probe design. However, although some valid data were obtained, at the end of the session tips were found to be short-circuited. Deposition of carbon on the insulating material in between and around the pins was found to be the cause of that problem. Although no temperature fluctuations measurements were made, results indicated that ion orbit effects do not appear to invalidate measurements. This was not clear since the distance between pins (0.25 mm) is smaller than the ion Larmor radius. Therefore, when the problem of carbon deposition is corrected, measurements of the temperature fluctuations are expected to be possible.

3.3.3.4. Small scale fluctuating sheared E×B flows

Recent gyro-fluid and fluid simulations have observed small scale fluctuating sheared ExB flows. These flows are driven by fluctuations and, according to these simulations, they can substantially reduce the turbulent transport. The effective sheared rate of fluctuating ExB flows is less effective than the slowly varying component in reducing the turbulent transport. This reduction in the effectiveness is particularly important when the ExB flow patterns changes in a time scale faster than the eddy turn over time. A rough estimation of the effective shearing rate of the fluctuating electric fields can be computed as

$$\tilde{\omega}_{E\times B} = \frac{(E_{radial})_{rms}}{B\lambda_c} f\left(\frac{\omega_f}{\Delta\omega_T}\right) \tag{3.1}$$

where ω_f and $\Delta\omega_T$ are the mean frequency of fluctuating radial electric field and the width of turbulent spectra, respectively, and λ_c is the radial correlation of fluctuations and B is the toroidal magnetic field. The function $f(\omega_f/\Delta\omega_T)$ takes into account the reduction of the effective shearing rate when the time scale of the fluctuating radial electric field is faster than the correlation time of fluctuations

$$f\left(\frac{\omega_f}{\Delta\omega_T}\right) \approx \begin{cases} 1 & if \quad \omega_f << \Delta\omega_T \\ 0 & if \quad \omega_f >> \Delta\omega_T \end{cases} \tag{3.2}$$

In the case of JET edge plasma conditions, $(E_{radial})_{rms} \approx 1000$ V/m, $\omega_f \approx \Delta\omega_T$ and the average radial correlation is in the range of 1 cm. Using expression (3.1), the effective decorrelation rates are close to the critical value to regulate turbulent transport ($\omega_{ExB} \approx 10^5$ s^{-1}), well below the L-H power threshold power in JET. A more accurate computation of the fluctuating ω_{ExB} shearing rate was done with Langmuir probe data from JET. The ω_{ExB} was computed as $\Delta\tilde{v}_\theta \Delta r$, being v_θ from the time delay of measurements between two Langmuir probes poloidally separated and measuring the fluctuating plasma potential. Although this computation has some limitations due to time resolution, the results agree, for different time scales, with the previous estimation (Fig. 3.6).

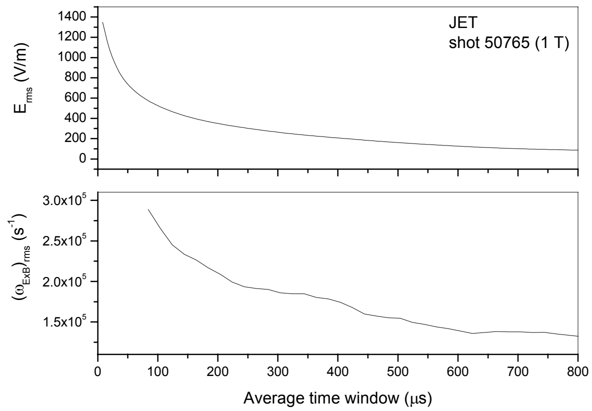

Fig. 3.6 - The E_{rms} and $(\omega_{ExB})_{rms}$ at different time scales show a similar evolution and good agreement with equation 3.1.

As was seen before, the effectiveness of this shearing rate on decorrelating transport events will depend of the time scale of the events. Once that we can not measure the function $f(\omega_f/\Delta\omega_T)$, the followed approach was try to see those effects on plasma behaviour. From JET Langmuir probe system is possible to have the simultaneous measurement of the turbulent ExB fluxes (Γ) at two radial positions separated 5 mm and the radial electric field (E_r) in the middle position. The signals of fluctuating potential and current saturation from the probes in the neighbourhood of 1 cm around his maximum penetration point were taken. After some manipulation it is possible to have the corresponding signal of E_r and Γ_{ExB}. Successive smoothes were applied to the signals and compute the correlation between E_r and Γ_{ExB} and the radial correlation between the two flux signals. This smooth of the signal corresponds to a filtering of the high frequency signals. The result of this calculation is presented in Fig. 3.7, where is possible to see the existence of a region of maximum correlation limited to some frequencies. In fact, it seems that in this region the turbulent flux is being regulated by the radial electric field once that, when the correlation between E_r and Γ_{ExB} tend to disappear, the radial correlation between fluxes decreases. This result was observed for different discharges obtained in different regimes and magnetic fields. The dependence of the radial correlation of the turbulent transport exhibits a different behaviour of the radial correlation of fluctuations. The dependence on the magnetic field gives the suspicious that certain scales of turbulence can scale with the Larmor radius while in the low frequency region this dependence is less evident. Further experiments are planned, including a comparison with the results obtained on a small device as ISTTOK, to put in evidence the role of the magnetic field and Larmor radius in these results.

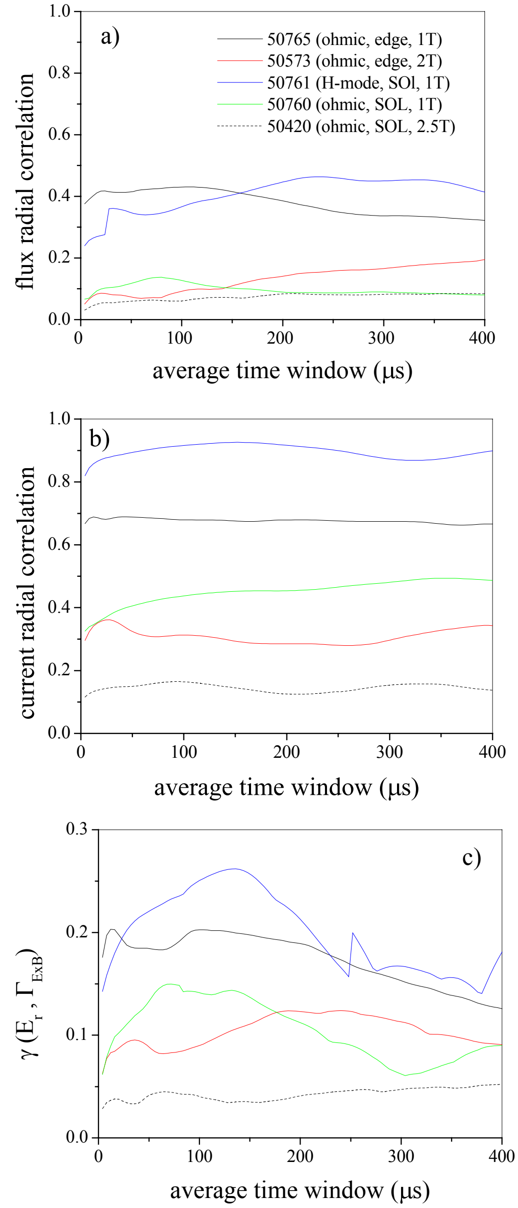

Fig. 3.7 - a) The turbulent flux radial correlation is bigger for higher frequencies showing a large dependence on magnetic field and plasma regime. b) The saturation current radial correlation exhibits distinct behaviour. c) The comparison with the coherence between electric field and turbulent flux is similar to flux radial correlation.

3.3.4. Microwave reflectometry

3.3.4.1. Introduction

The activities in this research area have been focussed in the following topics:

- Study of turbulence by microwave reflectometry
- Calibration and operation of the kG3 O-mode reflectometer

Following an international call for applications, Dr. Luís Cupido was appointed head of the project “Study of turbulence by microwave reflectometry”, by the EFDA JET Associate Leader.

3.3.4.2. Study of turbulence by microwave reflectometry

This project aims to enhance the radial access of the existing correlation reflectometer (kG8b) by including a new set of emitters-receivers in the range 75-110 GHz to probe along the internal transport barrier (ITB). The present configuration of this diagnostic provides only limited information because measurements can only be made at three radial positions simultaneously (corresponding to the frequencies: 75, 92-96 and 105 GHz). Also the waveguides show limitations with poor overall transmission and they can not be used above 110 GHz. This restricts the X-mode (high spatial resolution) operation to ITBs in discharges with the toroidal magnetic field below 3.4 T.

The project is divided in two phases:

- *Phase I*

  Consists of two emitter-receiver sets in the range 75-110 GHz. One of them will be set to the top of the band at 110 GHz and the second one will have a frequency in the range of the existing channels.

- *Phase II*

  Consists of one tunable correlation system able to probe along the ITB. A heterodyne detection system with the latest technology is required to overcome the expected poor performance of the waveguides and antennas. This system, by using broadband (full W band) devices both for power generation and signal reception, becomes in significant disadvantage with its narrow band counterparts usually constructed with powerful gunn or INPATT oscillators.

The following main activities have been performed in 2000:

- Participation of Dr. Luis Cupido in the definition of the project specifications and the content of the call for proposals and contracts.
- IST/CFN was chosen by the EFDA Culham Close Support Unit to develop the project, having the contracts been signed in the end of 2000.

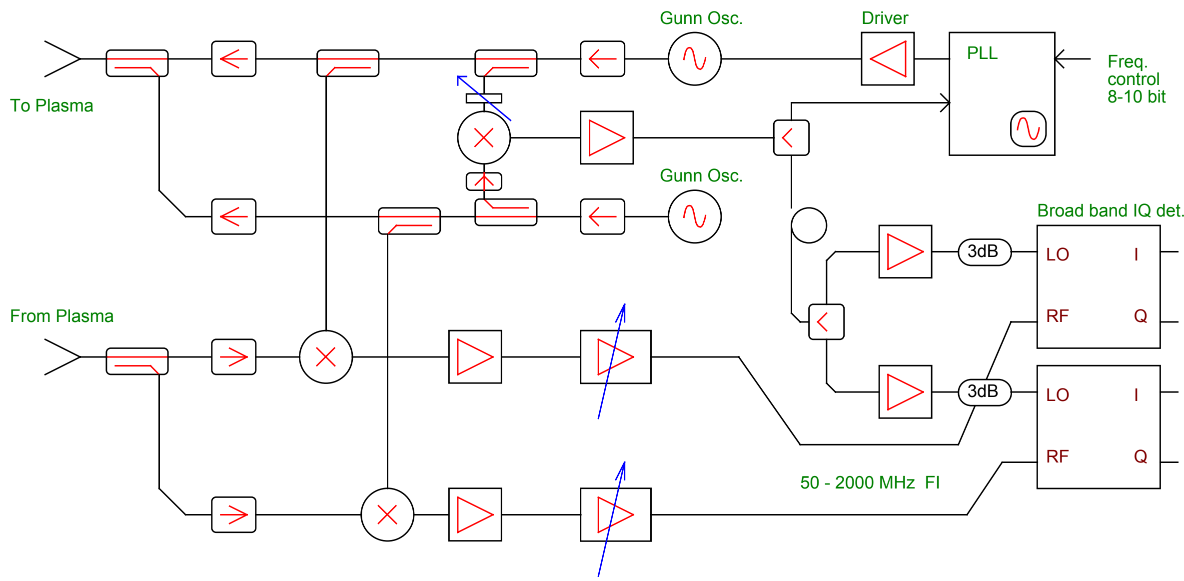

Fig. 3.8 - Block diagram of the proposed W band correlation channel for JET.

- IST/CFN has started the conceptual design of the components to be implemented on the JET correlation reflectometer

3.3.4.3. Calibration and operation of kG3 O-mode reflectometer

The work was developed under task force D during the C2 campaign and included:

- Operation of the microwave group diagnostics in the control room
- Development of calibration techniques for kG3 O-mode reflectometer.
- Some preliminary data analysis focusing the behaviour of low frequency fluctuations during ITB shots, using kG3 O-mode system, plus the correlation of fixed channels to measure radial correlation lengths (mostly at the edge of the plasma).

The use of an heterodyne phase and quadrature detection reflectometer implies the calibration of the system before any quantitative analysis can be performed. Ideally the system should deliver two signals with the same amplitude, no offsets and a phase difference of exactly 90º between them. Say, for instance, a cosine and a sine:

$$Q = A\sin(\theta) \tag{3.1}$$

$$I = A\sin(\theta + 90^\circ) = A\cos(\theta) \tag{3.2}$$

In the reality this is not the case as we get two signals that can be represented as follows:

$$Q = A\sin(\theta) + Q_0 \tag{3.5}$$

$$I = A \cdot A_{\mathrm{IQ}} \sin(\theta + \Phi) + I_0 \tag{3.6}$$

where I_0 and Q_0 are the offsets of the phase and quadrature signals respectively and A_{IQ} and Φ are the amplitude and phase imbalances between them. After straightforward manipulation, the calibrated signals can then be written as:

$$A\sin(\theta) = Q - Q_0 \tag{3.7}$$

$$A\cos(\theta) = \frac{I - I_0}{A_{\mathrm{IQ}}\sin(\Phi)} - \frac{Q - Q_0}{\tan(\Phi)} \tag{3.8}$$

In the remaining text this will be called the "homodyne signals". The two previous expressions can also be written as:

$$A = \sqrt{A^2\sin^2(\theta) + A^2\cos^2(\theta)} = \sqrt{(Q - Q_0)^2 + \left(\frac{I - I_0}{A_{\mathrm{IQ}}\sin(\Phi)} - \frac{Q - Q_0}{\tan(\Phi)}\right)^2} \tag{3.9}$$

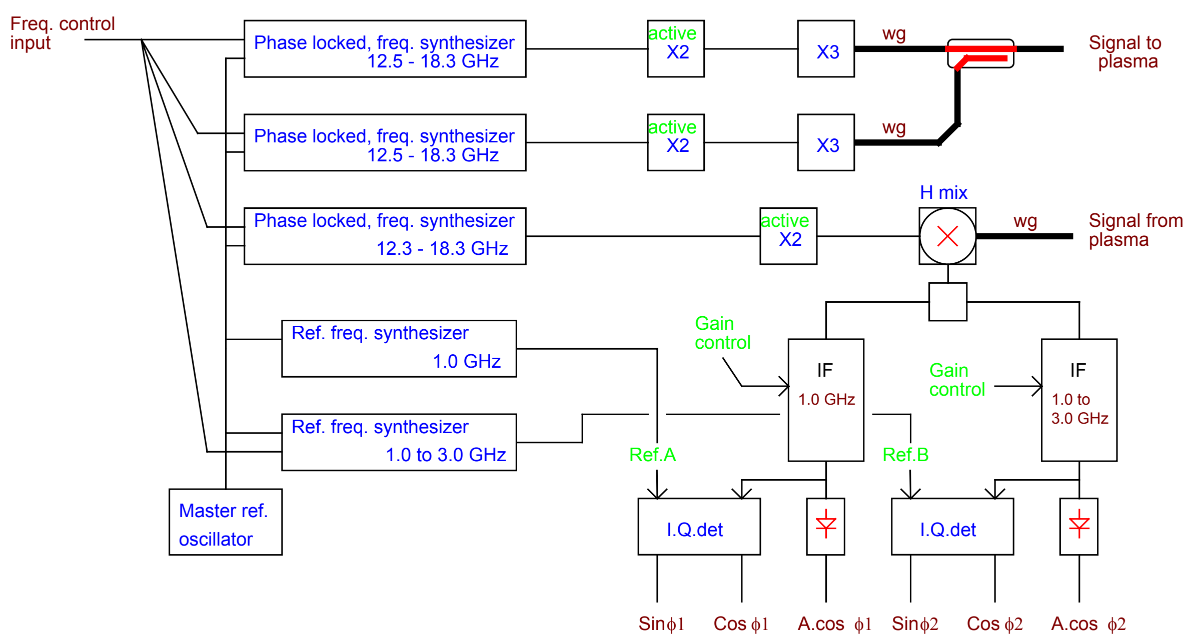

3.9 - Block diagram of the proposed W band tunable system for JET.

$$\theta = \arctan\left(\frac{A\sin(\theta)}{A\cos(\theta)}\right) = \arctan\left(\frac{Q-Q_0}{\dfrac{I-I_0}{A_{IQ}\,sin(\Phi)} - \dfrac{Q-Q_0}{tan(\Phi)}}\right) \quad (3.10)$$

which will be called the "heterodyne signals".

A computer code was developed to extract the phase and amplitude calibration factors (Φ and A_{IQ}) between the signals coming from the IQ detector of the radial correlation channels of the kG3 reflectometer (channel 4 – swept in frequency, against channel 10 – fixed in frequency), as a function of the probing wave frequency. The code is also prepared for the extraction of the offsets I_0 and Q_0, but this feature needs further hardware modifications to be performed. Once obtained, these factors will be used for software correction of the experimental data prior to its analysis.

The code analyses a series of fringes resulting from the same signal (swept in frequency) entering both the inputs of the IQ detector, with a suitable temporal delay between them. The code finds several fringes, by detecting zero crossings, and then applies Fourier techniques (three different methods for comparison of the results) to each fringe to extract the amplitude and phase imbalances between IQ detector output signals vs. their frequency[2] (different fringes correspond to different signal frequencies). The result (for each of the three methods) is then two numbers per fringe (phase and amplitude) per signal (I and Q). Each one of these arrays is then interpolated to the number of steps in frequency used in the first place.

As the calibrating signals were recorded using a digital oscilloscope (using an acquisition frequency of 25 kHz), the maximum number of samples acquired (2500) was too low for the total 2048 frequency steps needed[3], leading to poor statistics.

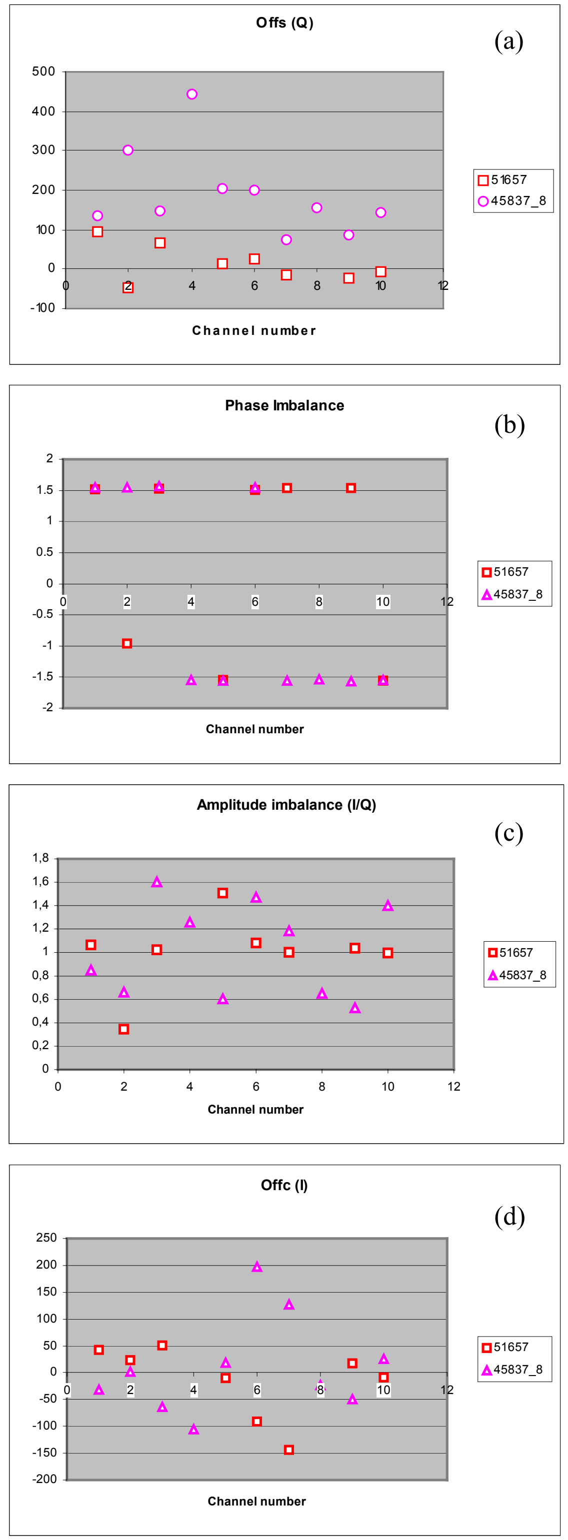

Fig. 3.10 – Plots of the calibration factors as a function of channel number corresponding to the data in tables 1. and 2. (a) Q signal offset – Q_0; (b) I signal offset – I_0; (c) amplitude ratio between I and Q signals – A_{IQ}; and (d) phase difference between I and Q signals – Φ.

[2] In reality, it is as a function of DAC value as the conversion to frequency is not yet implemented.

[3] The number of fringes that we get in a sweep is given by $\Delta f \Delta\tau$ where Δf stands for the frequency range swept and $\Delta\tau$ is the temporal delay between the two input signals. In our case $\Delta f \approx 1e9$Hz and $\Delta\tau \approx 150e-9$s, so $\Delta f \Delta\tau \approx 150$. We need ~2000 steps in frequency to get something like ~10 points on average per fringe.

The next step to take should involve the use of a different acquisition system in order to fulfill the need for more samples per calibration. Also very important are the kG3 hardware modifications necessary to determine the correction for the offsets in the IQ signals.

To calibrate the channels 1-10 (except 4), another computer code was also developed with the objective to extract the same correction factors (phase, amplitude and offset). Its basis is similar to the one of the previous code mentioned, with the differences being due to the fact that probing frequency of the microwaves is now constant. Only one Fourier method (the first) is now used.

To produce the fringes on the output of the IQ detector we now use two signals with slightly different frequencies entering it (in our case we used 10.7 MHz and 10.6987 MHz). Since the frequency is constant we now apply the Fourier to all the fringes produced, rather that to each fringe at a time. In this case, the offsets for I and Q signals can also be determined by calculating the mean value of each them, as the signals are now stationary in time. The result is 36 numbers: 4 for each of the 9 channels (I_0, Q_0, A_{IQ} and Φ). These numbers are then used by the data analysis codes that treat correlation reflectometry data namely they are needed for the measurement of the radial correlation lengths. We acquired one calibration signal for these 8 channels, using the CATS data acquisition system, so we have good statistics in this case (acquisition frequency of 250 kHz).

Comparison of the results obtained from this calibration acquisition (#51657) with an older one (#45837 and #45838) showed big variations on the offsets and amplitudes, which is probably a consequence of changes in the system settings (for instance, changes in the gains of the amplifiers). On the other hand, the phase seems to be fairly constant (Fig. 3.11) (except for channel 2 where a fault must have happened for shot #51657). At this point it is important to stress the need for more acquisitions in similar conditions to further investigate the stability of the system.

Fig. 3.11 presents the coherence between two fixed frequency channels (ch. 2 and 3) calculated using "homodyne" (sine and cosine) and "heterodyne" (phase and amplitude) signals. We can see that there are differences between them. Actually, the coherence calculated from the phase and amplitude signals is more sensitive to the calibration factors and so more difficult to obtain. Namely, the phase, which is the most interesting quantity to study (it is free from the amplitude variations of the reflected signal due to effects like difraction and refraction or gradient changes in the plasma), has a strong dependence on the offsets of the signals. For this reason we also use the "homodyne signals", which are less dependent on the calibration.

For each time, the "homodine" coherence is given by the maximum of both curves. The reason is that when we are in the linear part of a cos(x) function (high coherence) this corresponds to the non-linear part of a sine(x) function (low coherence), and vice-versa. That is why the two "homodyne" coherence curves are "out of phase" during most of the time.

Also presented is the localization of the reflecting layers for the different channels (Fig. 3.12) from the KE3 LIDAR Thomson Scattering System. We see that we are looking at the plasma edge and that the reflecting layers are, according to this plot, almost superimposed. In reality, one should look at the

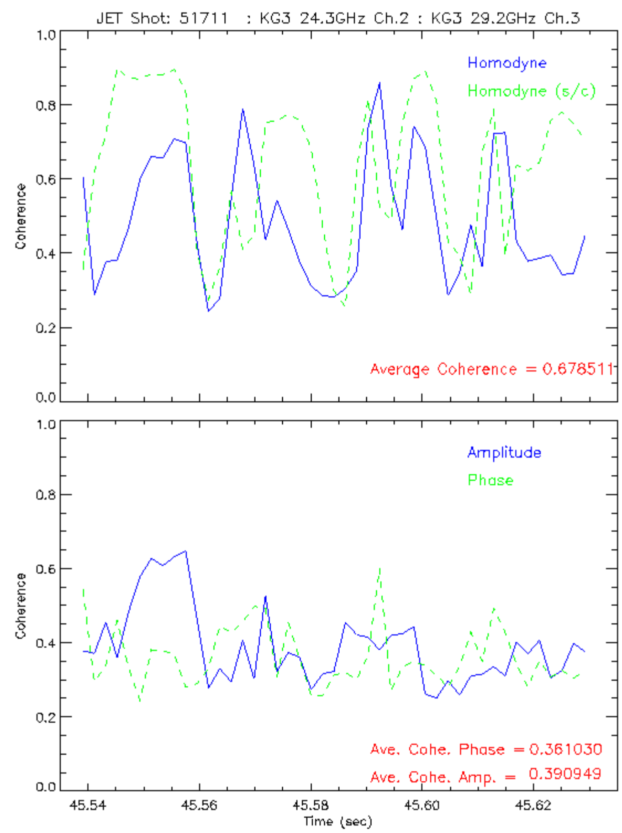

Fig.3.11 – Coherence between channels 2 and 3 calculated using both the (a) "homodyne signals" and (b) "heterodyne signal

information from KE9, the divertor LIDAR, that gives better results for this region of the plasma (after folding the data points to the mid-plane along the flux surfaces).

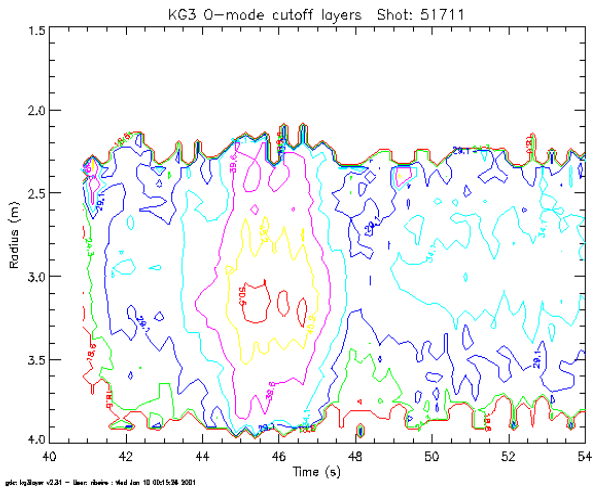

Fig. 3.12 – Temporal evolution of the reflecting density layers for KG3 reflectometer as measured by KE3, the LIDAR Thomson Scattering.Legend: ch.1→18.6GHz; ch.2→24.3GHz; ch.3→29.1GHz; ch.4→34.1GHz; ch.5→39.6GHz; ch.6→45.2GHz; ch.7→50.5GHz; ch.8→57.7GHz; ch.9→63.9GHz; and ch.10→69.6GHz

3.3.5. Control and data acquisition

The following main activities were performed in 2000:

- Conceptual study of the control and data acquisition system for the JET correlation reflectometer
- Beginning of the development of the VME modules for control and transient recording.

3.3.6. Thomson scattering diagnostics

The following main activities have been made:

- Training in the routine operation of the diagnostics of the D1 and D2 Groups.
- Collaboration in the re-alignment of two Thomson Scattering Diagnostics (kE3 and kE9).
- Participation in meetings of the High Resolution Thomson Scattering Working Group.
- Improvement of a program for the analysis of the JET Thomson Scattering data by including a non-linear binning technique of the CCD surface.

3.4. MANAGEMENT

IST/CFN has collaborated on the management of the use of the JET Facilities by the EFDA Associates in the following manner:

- Prof. Fernando Serra is member of the EFDA Sub-Committee for JET (JSC) (six meetings in 2000).
- Dr. Duarte Borba belongs to the staff of the Close Support Unit (CSU) to the EFDA Associate Leader for JET, since April 1st 2000.
- Profª. Maria Emília Manso was (is) member of the Ad-Hoc Group for Phase I (Phase II) evaluation of the JET Enhancement Project (four meetings in 2000).
- Prof. Fernando Serra is member of the Ad-Hoc Group for the Assessment of the diagnostics requirements for the JET Enhancement Project (three meetings in 2000).
- Prof. H. Fernandes and Mr. P. Varela belong to the Remote Participation Users Group (two meetings in 2000).
- Mrs. Nave was Liaison Officer between the Portuguese Association and the JET Joint Undertaking within the scope of the Winding-up Contract for the analysis of the 1999 JET data (two meetings in 2000).
- Mrs. Maria Fernanda Pinto is the IST/CFN contact person for administrative matters.